SANDIA REPORT
SAND2020-10208
Printed September 2020

Sandia National Laboratories

Resistive heating in an electrified domain with a spherical inclusion: an ALEGRA verification study

Angel E. Rodriguez, Christopher M. Siefert, and John H. J. Niederhaus

Prepared by
Sandia National Laboratories
Albuquerque, New Mexico
87185 and Livermore,
California 94550

Issued by Sandia National Laboratories, operated for the United States Department of Energy by National Technology & Engineering Solutions of Sandia, LLC.

Available to DOE and DOE contractors from
U.S. Department of Energy
Office of Scientific and Technical Information
P.O. Box 62
Oak Ridge, TN 37831

Telephone: (865) 576-8401
Facsimile: (865) 576-5728
E-Mail: reports@osti.gov
Online ordering: http://www.osti.gov/scitech

Available to the public from
U.S. Department of Commerce
National Technical Information Service
5301 Shawnee Rd
Alexandria, VA 22312

Telephone: (800) 553-6847
Facsimile: (703) 605-6900
E-Mail: orders@ntis.gov
Online order: https://classic.ntis.gov/help/order-methods/

ABSTRACT

A verification study is conducted for the ALEGRA software, using the problem of an electrified medium with a spherical inclusion, paying special attention to resistive heating. We do so by extending an existing analytic solution for this problem [8] to include both conducting and insulating inclusions, and we examine the effects of mesh resolution and mesh topology, considering both body-fitted and rectangular meshes containing mixed cells. We present observed rates of convergence with respect to mesh refinement for four electromagnetic quantities: electric potential, electric field, current density and Joule power.

ACKNOWLEDGEMENTS

This study was sponsored by the CCDC Army Research Laboratory (ARL). Thanks to Misha Grinfeld (CCDC ARL) and Tom Voth (Sandia) for technical collaboration and review.

CONTENTS

LIST OF FIGURES

LIST OF TABLES

This page left blank

ACRONYMS AND DEFINITIONS

Abbreviation	Definition
2D	Two dimensional
3D	Three dimensional
ALEGRA	Arbitrary Lagrangian-Eulerian General Research Application
MHD	Magnetohydrodynamics

1. INTRODUCTION

The ability of the ALEGRA software (Arbitrary Lagrangian Eulerian Research Application) [1] to compute Joule heating accurately in mixed-material elements is important for all of its magnetohydrodynamics (MHD) use cases that use Eulerian meshes. These use cases include pulsed power systems such as exploding wires [2] and electromagnetically launched flyer plates [3]. Mixed-material elements are problematic because the evolution of the electromagnetic field is computed in ALEGRA without regard to subgrid material interfaces. That is, appropriate interface conditions on the electromagnetic fields are not imposed, nor are even representable by the finite element spatial discretization used by ALEGRA, unless the interface should happen to fall on a cell boundary. Instead, mixed-material MHD simulations on Eulerian meshes rely on "averaging out" the spatial variation of the electrical conductivity to in order to compute the orientation of electromagnetic fields near interfaces. Without extensive changes to the spatial discretization, this is unavoidable [4]-[5].

Maxwell's equations would ideally be solved in the vicinity of material interfaces by imposing interface conditions on the electromagnetic field: continuity across the interface of the normal component of the magnetic induction $\vec{B}$, and of the tangential component of the magnetic field $\vec{H}$. Since this cannot be done in the Eulerian, mixed-material meshes of typical ALEGRA MHD simulations, some systematic error is inherent to these calculations. Additionally, some error enters the solution through the approximate values of the electrical conductivity in the mixed-material elements. These errors can be expected to affect the electric potential, electric field, electric current density, and magnetic field [6]-[7].

By extension, these errors would also affect the computed rate of Joule heating. This is the Ohmic or resistive effect whereby material with a finite electrical conductivity gains thermal energy due to imposed fields that draw an electric current through it. Since Joule heating can affect the electrical conductivity strongly via phase changes, very large errors can arise very rapidly. These errors are of concern for MHD applications of the ALEGRA software and should be quantified, along with the underlying errors in the electromagnetic fields themselves.

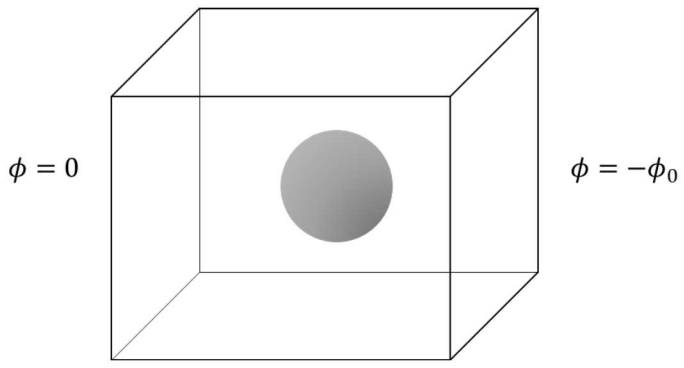

Figure 1: Conceptual layout of the sphere inclusion verification problem.

A verification problem has been created previously to study Joule heating and other aspects of transient magnetics models rigorously with mixed-material elements [8]. This problem is shown conceptually in Figure 1 and consists of a conducting domain, with a voltage ϕ_0 applied across it, within which an insulating spherical inclusion distorts the electromagnetic fields and flow of current. Simple closed-form analytic solutions were derived in Reference [8] for the steady-state electric potential, electric field, current density, and local rate of Joule heating. That improved upon the previous Joule heating analyses of Elliott and Larsson [9] and Holst *et al.* [10] by allowing multiple materials, and that of Rienstra [11] by avoiding a problem involving a corner and the associated singularity.

In the present work, we extend the verification analysis of Reference [8] for this problem to include both conducting and insulating inclusions, and examine the effects of mesh resolution and mesh topology (rectangular versus body-fitted). In Section 2 of this report, details of the analytic solutions are outlined. ALEGRA simulation configurations for the cases to be studied are described in Section 3, and their results are examined in Section 4. The complete verification error analysis for Joule heating and electromagnetic fields and potential appears in Section 5.

2. SUMMARY OF ANALYTIC SOLUTION

In Reference [8], we evaluated exact solutions for an insulating sphere in a conducting medium with a uniform current density. An exact solution was derived in an explicit, closed form for the system with fixed current applied to a linear isotropic electroconducting material with a spherical (Equations 32-37) or circular-prismatic (Equations 57-60) inclusion. For convenience and brevity, we choose to study the case of a sphere with radius R, and chose $\hat{x}$ as the direction of the fixed current imposed at the far boundaries. In this case, if the domain has a fixed electrical conductivity, then Ohm's law implies that boundary conditions prescribing the far-field current density J_{far} at infinity are interchangeable with an ambient electric field E_{far}. If the material conductivity is isotropic, then cylindrical symmetry is ensured.

Within these limitations, the solution reduces to simpler forms. For constant, isotropic conductivities σ_{in} inside the inclusion and σ_{out} outside (in the ambient matrix), the solution is axisymmetric. Choosing $\hat{x}$ as the direction of the ambient electric field, the solution fields are functions of only x and r, the normal distance from the x-axis. For any radial location $\vec{\rho}$ inside or outside the sphere (measured with respect to its center), the electric potential reduces to the following equations, normalized to the undisturbed potential field, $E_{far}x$:

$$\frac{\phi(r,x)_{in}}{E_{far}x} = \frac{-3\sigma_{out}}{\sigma_{in}+2\sigma_{out}}, \qquad \rho \le R \tag{1.1}$$

$$\frac{\phi(r,x)_{out}}{E_{far}x} = \left(\frac{\sigma_{in}-\sigma_{out}}{\sigma_{in}+2\sigma_{out}}\frac{R^3}{\rho^3}-1\right), \qquad \rho \ge R \tag{1.2}$$

The solution for electric field ($\vec{E} = -\nabla\phi$) can be reduced to these two normalized equations:

$$\frac{\vec{E}(r,x)_{in}}{E_{far}} = \frac{3\sigma_{out}}{\sigma_{in}+2\sigma_{out}}\hat{x}, \qquad \rho < R \tag{1.3}$$

$$\frac{\vec{E}(r,x)_{out}}{E_{far}} = \hat{x} + \frac{\sigma_{in}-\sigma_{out}}{\sigma_{in}+2\sigma_{out}}\frac{R^3}{\rho^3}\left(-\hat{x}+3\frac{x}{\rho}\left(\frac{\vec{x}}{\rho}+\frac{\vec{r}}{\rho}\right)\right), \quad \rho > R \tag{1.4}$$

Notice that $x/\rho = \sin\theta$ and $r/\rho = \cos\theta$ where θ is the angle from $\vec{x}$ to $\vec{\rho}$. Hence, $\vec{x}/\rho + \vec{r}/\rho = \hat{\rho}$ (the unit vector).

The Ohmic current density field is simply $\vec{J} = \sigma\vec{E}$. Split explicitly by region and normalized to $J_{far} = \sigma_{mat}E_{far}$, we get the following equations:

$$\frac{\vec{J}(r,z)_{in}}{J_{far}} = \frac{3\sigma_{in}}{\sigma_{in}+2\sigma_{out}}\hat{x}, \qquad \rho < R \tag{1.5}$$

$$\frac{\vec{J}(r,z)_{out}}{J_{far}} = \frac{\vec{E}(r,x)_{out}}{E_{far}}, \qquad \rho > R \tag{1.6}$$

We introduced field distortion factors due to the sphere's presence that depend only on the conductivity of the inclusion (σ_{in}) relative to the ambient (σ_{out}), as follows:

$$D_{in} = \frac{3\sigma_{out}}{\sigma_{in} + 2\sigma_{out}} \tag{1.7}$$

$$D_{out} = \frac{\sigma_{in} - \sigma_{out}}{\sigma_{in} + 2\sigma_{out}} \tag{1.8}$$

It's clear in Equations 1.2 and 1.4 that the outside field distortions caused by the inclusion decay as $(R/\rho)^3$.

3. FINITE ELEMENT SIMULATION SETUP

As described in References [1], [6], and [7], ALEGRA is a multiphysics, multimaterial finite-element simulation code that can be used to model resistive magnetohydrodynamics and electromechanics in two or three dimensions (2D or 3D). Similarly to the previous verification studies in References [6] and [7], here we use only the "transient magnetics" module from the 3D electromagnetics portion of the code, leaving any concept of material motion or mechanics out of the simulation. In this portion of ALEGRA, the transient eddy-current diffusion equation is solved using implicit time integration on a 3D mesh of hexahedral finite elements. The spatial discretization places magnetic flux on element faces and electric field circulation on elements edges, forming a "mimetic" or "compatible" discretization that allows the physical and mathematical properties of Maxwell's laws to be preserved more rigorously. This discretization has been described and evaluated elsewhere.

The simulation is created as an initial boundary value problem in Cartesian (x, y, z) space. We chose to have the far-field electric field and current density lie along the x-axis. The electrical conductivity σ is specified everywhere in the domain, associated with the local material composition. The $x = 0$ plane of symmetry is defined as ground ($\phi = 0$), and a fixed driving voltage $\phi_0 = -E_{far} x_{max}$ is applied to the maximum-x boundary for all time. On these specified-voltage surfaces, the electric field is constrained to be everywhere normal to the boundary: $\vec{E} \times \hat{n} = 0$. On the lateral $(-y, +y, -z, +z)$ boundary surfaces, the electric field is constrained to be tangent to the boundary: $\vec{E} \cdot \hat{n} = 0$.

With exterior boundaries sufficiently far from the inclusion, this sets up a uniform electric field equal to E_{far} outside of the region distorted by the inclusion. The electric current is initially zero everywhere. The simulation runs until a steady-state flow of current is reached, and this solution is compared to the analytic solution described above. A constant time step size of 0.5 μs is used, but for these cases, the steady state is reached in the first time step.

Two simplifications are made to the model here. First, we apply the "low magnetic Reynolds number" ("low R_m") approximation in ALEGRA [12]-[14]. In this approximation, the contribution to the current density due to a time-changing magnetic field is assumed to be small relative to the contribution due to the electric field gradient. The magnetic field can then be dropped from the system completely, and instead of the eddy-current diffusion equation, only this equation is solved on each timestep:

$$\nabla \cdot \sigma \nabla \phi = 0 \tag{2.1}$$

This equation is much less computationally expensive to solve and allows the use of more convenient electric-potential boundary conditions ("potential drive") for the present case. The electric field is then derived from this approximation as $\vec{E} = -\nabla \phi$. Without this approximation, boundary conditions on the magnetic field would be required. This approximation still allows one to calculate Joule heating.

The second approximation is that axial and lateral symmetry is applied when choosing the domain for simulation. The "low R_m" approximation is only available in 3D in ALEGRA, so the simulation cannot take advantage of the inherent axisymmetry of the problem. Instead, symmetry about all three coordinate-aligned midplanes of the spherical inclusion is assumed. Thus, the simulation domain need only enclose a 1/8 sector of the sphere inclusion, along with the outer region extending to one of the far boundaries.

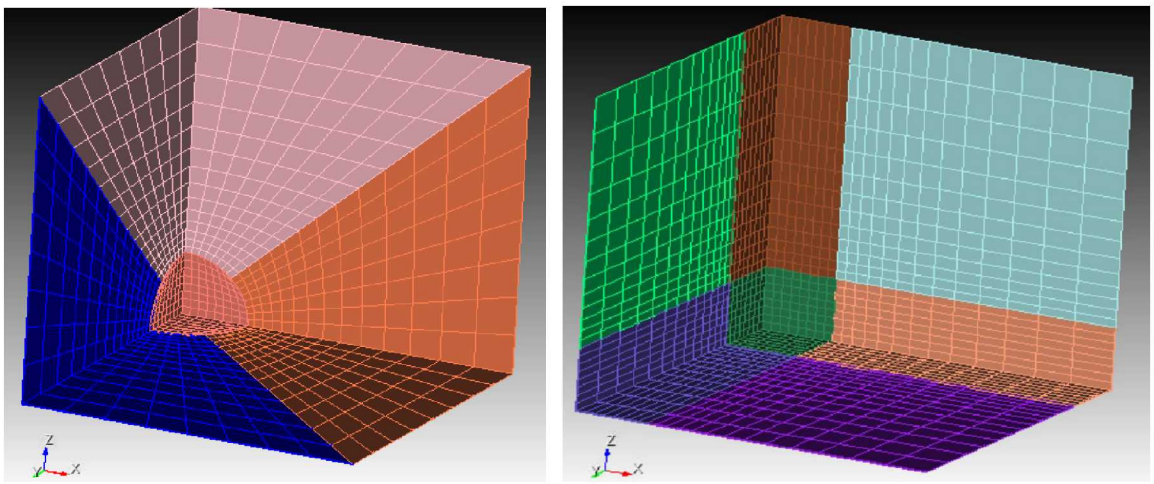

Figure 2: Computational grids: Conformal Grid at left; Brick Grid at right

Two hexahedral meshes are generated for the simulations: a conformal grid and a brick grid. The conformal grid has block boundaries conforming to the spherical surface of the inclusion, so every element contains only pure material. Mixed-material elements are completely avoided. A coarse version of this mesh is shown in Figure 2 on the left. Numerical errors (details below) at high enough resolution become comparable to boundary condition errors at modest distances. To avoid this, the $+x$ boundary of the mesh is additionally made conformal to equipotential curves from the exact solution, and the $+y$ and $+z$ boundaries are made conformal to the electric field lines from the exact solution. This is done even for the nominally rectangular "brick" grid. These adjustments to the mesh are on the order of microns in magnitude for the geometry used here. They are not visible in this macroscopic view of the mesh, where the boundaries appear to be flat. Without these subtle adjustments, a prohibitively large distance may be required between the exterior boundaries and distorted-field region around the inclusion. With these adjustments, the boundary conditions can be made correct within numerical accuracy, even for relatively close boundaries.

A simpler brick grid is more typical of routine production ALEGRA simulations, because it is easier to generate. However, mixed-material elements are then unavoidable. The conformal grid, on the other hand, is less practical to generate, but provides much better accuracy. Comparisons then provide insight into and metrics of the effect of mixed material elements on the quality of computed results. Both grids above are at a resolution of 8 elements per radius, and both relax the mesh interval linearly toward the far boundaries.

4. FINITE ELEMENT SOLUTIONS

Using the meshes and simulation settings described above, ALEGRA simulations are performed for insulating and conducting inclusion cases. We use a sphere radius $R = 1$ m, with the coordinate origin at its center, and the three exterior boundaries at 5 meters. A driving voltage $\phi_0 = -500$ V at $x = 5$ m effectively imposes an exterior electric field $E_{far} = 100$ V/m. The exterior has a conductivity of 1 S/m, and the inclusion has either 10^{-9} or 10^{9} S/m, representing a near-perfectly insulating or conducting sphere, respectively.

The mesh resolution is designated by the number of elements N spanning the sphere radius. A linear bias extends outward from the sphere surface to the boundaries. The meshes shown in Figure 2 are for $N = 8$ (elements per radius) for legibility, but calculations are performed for resolution as high as $N = 64$.

The results of the ALEGRA simulations with conformal grids at $N = 64$ are shown in Figure 3. This view shows the $z = 0$ plane, reflected about the other two symmetry planes in order to visualize four solution parameters. Included in this plot is the volumetric rate of Joule heating, $\vec{J} \cdot \vec{E}$. This quantity has units of power per unit volume, and it describes the rate at which heat is deposited locally due to current flow through material with finite conductivity. The ALEGRA simulations here are done with Joule heating disabled, to preserve the stationary nature of the final solution. (Thermal conduction is also excluded.) Instead, $\vec{J} \cdot \vec{E}$ is computed here as a post-processing step for comparison to the analytic solution.

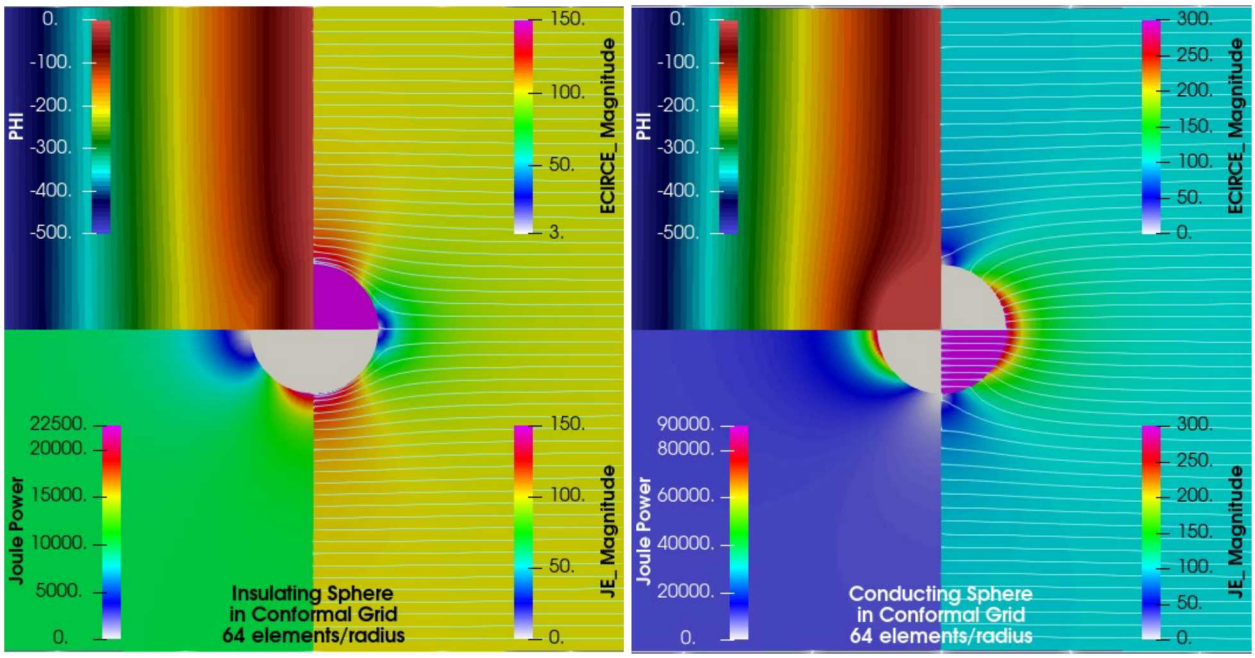

Figure 3: ALEGRA solutions computed on a Conformal Grid, where PHI is the electric potential, ECIRCE is the electric field and JE is the current density.

Shown in Figure 3 are these variables from the ALEGRA simulation (in clockwise order from the top left): electric potential ϕ, electric field magnitude $|\vec{E}|$, current density magnitude $|\vec{J}|$ and rate of Joule heating, $\vec{J} \cdot \vec{E}$. (These are noted as PHI, ECIRCE Magnitude, JE Magnitude, and Joule Power in the figure.) For the electric field and current density, streamlines of the vector fields are overlaid as well. For the electric potential, a discrete stepped color mapping is used so that equipotential lines are visible as boundaries between color gradations.

For each of these two cases, the ALEGRA solution is visibly indistinguishable from the analytic solution. For the insulating sphere, current streamlines diverge around the inclusion, and equipotential lines bunch up into it. For the conducting sphere, equipotential lines diverge around the inclusion, and current streamlines bunch up into it. In both cases, the electric field and current density are uniform within the inclusion, and the electric potential is a function of x only, as expected from the analytic solution discussed above.

We have confirmed that, under refinement of the mesh, the interior field magnitudes and the maximum exterior values approach the analytical values for the two cases: $E = 1.5E_{far}$ for the insulating sphere, and $J = 3J_{far}$ for the conducting sphere. The Joule heating maxima approach the analytical limits for both cases. For the insulating sphere, it approaches $\sigma\left|\vec{E} \cdot \vec{E}\right| = 1.5^2\ \sigma_{out}E_{far}^2 = 22.5$ kW/m^3 concentrated in a region immediately exterior to the "equator" of the insulating sphere. For the conducting sphere, it approaches $3^2\ \sigma_{out}E_{far}^2 = 90$ kW/m^3 concentrated just outside the "pole" of the conducting sphere.

Notice that in the limit $\sigma_{in} \ll \sigma_{out}$ (perfect insulator), $J_{in} \to 0$ but $E_{in} \to 1.5\, E_{out}$. Conversely, in the limit $\sigma_{in} \gg \sigma_{out}$ (perfect conductor), $E_{in} \to 0$ but $J_{in} \to 3\, J_{out}$. Both of these results are compatible with Equations 1.3 and 1.5. The electric field is discontinuous (in the interface normal direction) at the sphere surface. It is only definable as the limit of ratios of one-sided differences. However, continuity of the current density is never violated.

The numerical solutions for the brick grid are shown in Figure 4 using the same format as Figure 3. Color bars are modified to indicate regions where the analytic maximum has been exceeded, by shading them pink. We see that across all of the interior of the sphere, and in elements on its surface, the electric field magnitude (insulating case) and current density magnitude (conducting case) both exceed the analytic value. The mixed-material elements are also evident near the sphere surface as tiny irregularities. However, the qualitative features of the solution are preserved, and the results are approximately correct away from the surface, exterior to the sphere. To quantify these observations, we define error norms so that a convergence analysis can be conducted.

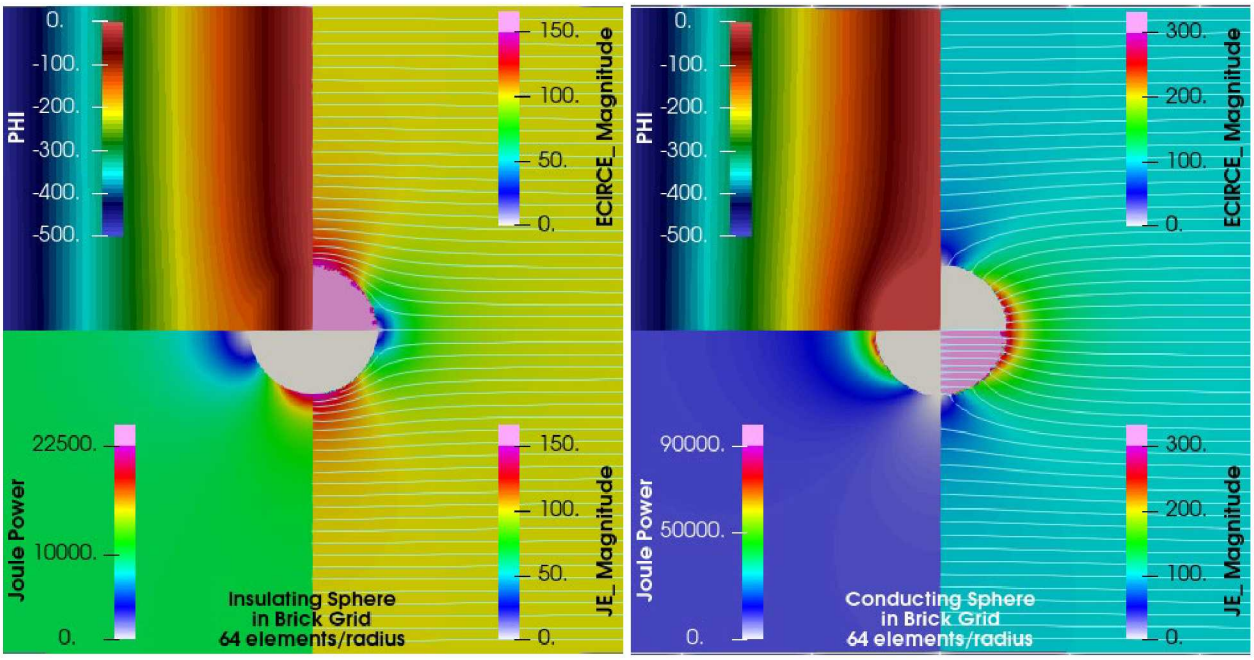

Figure 4: ALEGRA solutions computed on a Brick Grid, where PHI is the electric potential, ECIRCE is the electric field and JE is the current density.

5. ERRORS IN THE FINITE ELEMENT SOLUTIONS

5.1. Error norms

For a global error metric, we define the normalized second-order error norm for any solution field, F, as follows:

$$L_2(F) = \sqrt{\frac{\int |F_{calc} - F_a|^2 dV}{\int F_a^2 dV}} \tag{5.1}$$

where F_{calc} is the calculated field and F_a is the analytical (exact) solution at any position in the domain. This definition of the L_2 norm is consistent with the continuous and discrete L_2 error norms defined in References [15]-[17], except that the denominator has been introduced in Equation 5.1 to obtain a normalized, dimensionless error. The volume integrals are evaluated over the entire domain for global metric, and calculated discretely as the sum of contributions in each element. For vector fields ($\vec{E}$ and $\vec{J}$), the difference (error) is also a vector, but only its magnitude is considered here.

For the problem we are considering, the volume integrals of the fields (ϕ, $\vec{J}$, $\vec{E}$, and $\vec{J} \cdot \vec{E}$) in the denominator of equation 5.1 are unbounded as one chooses farther and farther boundaries. However, the distortions of the fields due to the inclusion decay as $1/\rho^3$, so their volume integrals are finite even to infinity. The error norm of the field distortion becomes

$$L_2(F_d) = \sqrt{\frac{\int |(F_{calc} - F_{far}) - (F_a - F_{far})|^2 \, dV}{\int |F_a - F_{far}|^2 \, dV}} \tag{5.2}$$

The numerator is unchanged, but the integral in the denominator is now finite even for infinitely distant boundaries. The integrand decays as $1/\rho^6$. This metric is insensitive to the choice of domain limits beyond a modest distance.

Separating the numerator and denominator, Equation 5.2 becomes this:

$$\mathcal{N} = \int |F_{calc} - F_a|^2 \, dV \qquad \mathcal{D} = \int \left|F_a - F_{far}\right|^2 \, dV \qquad L_2(F_d) = \sqrt{\frac{\mathcal{N}}{\mathcal{D}}} \tag{5.3}$$

The volume integrals are calculated discretely as the sum of contributions in each element. The calculated electric potential, ϕ, is linearly interpolated between nodes. However, all element-centered variables in ALEGRA ($\vec{J}$, $\vec{E}$, and $\vec{J} \cdot \vec{E}$ here) are spatially constant across the element [18]. The elementary error for these variables is the element-centered value, F_{el}, minus the analytical value,

$F_a(\vec{r})$, which may vary across the element. The elementwise contribution to the numerator integrand in Equation 5.3 therefore requires its own integration, written as

$$\delta_2(F) = \int_{el} |F_{el} - F_a(\vec{r})|^2 dV \tag{5.4}$$

This integral is evaluated in each element using Gaussian quadrature with $3^3 = 27$ points. (A single-point quadrature would degenerate to the simple differences at element centers.) The global numerator is then calculated discretely as

$$\mathcal{N} = \sum_{el} \delta_2(F) \tag{5.5}$$

where the sum is taken over all elements. The integral in the denominator can be evaluated discretely using the same numerical process.

5.2. Spatial distribution of errors

For visualization of the spatial distribution of errors, we plot the volume-average element errors, defined as follows:

$$\epsilon_{el}(F) = \sqrt{\delta_2(F)/V_{el}} \tag{5.6}$$

For element-centered fields, the volume-average errors are normalized by the ambient or "far" value. For example, the $\vec{J} \cdot \vec{E}$, error has units of W/m^3, which can be normalized by , $J_{far}E_{far}$.

For node-centered ϕ, we plot the simple difference $\phi_{calc} - \phi_a$ at each node, which can be positive or negative, and is interpolated between nodes. There is no finite "far" value of ϕ, so we normalize by $E_{far}R$.

Error distributions for conformal grids at $N = 64$ are seen in Figure 5. We scale all errors by far-field values, as if we had chosen $E_{far} = 1$ and $J_{far} = 1$. Hence all errors are dimensionless and we expect to see values much less than one.

We see in Figure 5 that the largest errors are concentrated near the sphere surface, and decay away from the sphere. The scaled error magnitudes on the conformal grids at $N = 64$ are exceedingly small for the electric potential – on the order of 0.01%. The other variables mostly show errors on the order of a few percent in this normalization.

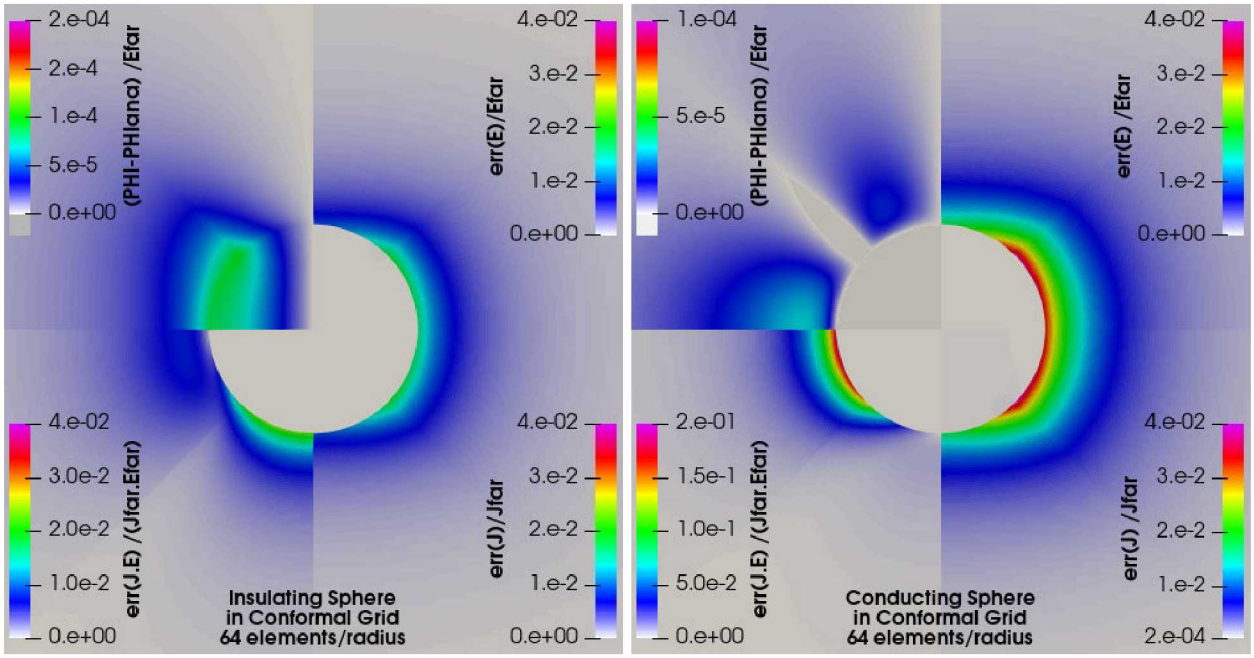

Figure 5: Error distributions for a Conformal Grid.

The exception in the conformal grids is the Joule heating in the conducting case, which shows maximum errors on the order of 10% of the far-field value, even in the absence of mixed-material elements. For perspective, the analytical maximum $\vec{J} \cdot \vec{E}$ value is $2.25\, J_{far} E_{far}$ for an insulating sphere, and $9\, J_{far} E_{far}$ for a conducting sphere. We note that the errors can have either sign—overheating or underheating—even though $\epsilon(F)$ is always positive. We also note that errors are preferentially located near the sphere surface in both cases. The presence of these errors is remarkable for several reasons. On one hand, these errors are expected, because ALEGRA does not allow for the appropriate interface conditions on the normal and tangential components of the electromagnetic fields to be imposed locally in the domain interior. This was also observed and discussed in Reference [7]. (Such conditions would be impractical for MHD simulations with motion, particularly for Eulerian meshes.) On the other hand, in Reference [7], similar errors were attributed to mixed-material elements. But in this mesh, there are no mixed material elements. Thus, we observe that even with pure materials, and a mesh that is conformal to interfaces, there are considerable errors in the local rate of Joule heating.

Extending this to the brick grid (with mixed-material elements), we see much greater errors than were seen in Reference [8], or in the conformal-grid cases. These are shown Figure 6 for the analogous $N = 64$ simulations. Color bars are modified, shading in pink those regions where the error magnitudes are particularly large. In these plots we see that the errors are especially large in or near the mixed-material elements, and they extend into the pure-material elements as well. Unlike the conformal-grid solutions, here we see errors on the order of a few percent in the insulating case for all variables, including ϕ. For the conducting sphere, the errors are considerable – reaching as large

as 10% or more of the far-field value for the electric field, current density, and Joule power, even on this relatively fine mesh.

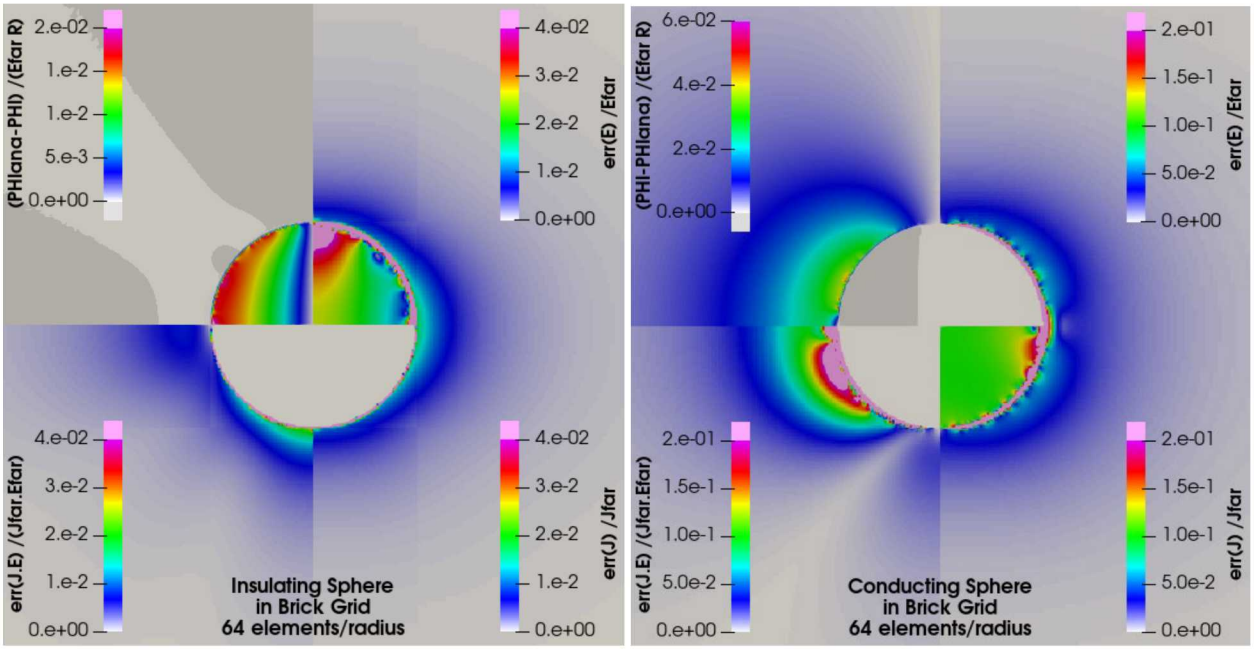

Figure 6: Error distributions for a Brick Grid.

These errors are concerning in MHD simulations, where electromagnetic fields are coupled to the dynamics and thermodynamics of moving media. Particularly in simulations with materials that may act as nonlinear thermistors, the local heating can affect the local electrical conductivity, which may lead to intense, localized Joule heating that is spurious. Therefore, the behavior of these errors under mesh refinement needs to be understood.

5.3. Global error analysis with mesh refinement

To complete a global measure of the error, we must evaluate the denominator in Equation 5.3. It is not straightforward to evaluate the volume integral of the disturbances outside the sphere analytically. Hence, we evaluate the denominator numerically from the most accurate simulation (conformal grid at highest resolution).

We find that for far enough boundaries, the contributions to the integral outside the finite domain can be neglected. The values shown in Table 1 are calculated using the conformal grid with $N = 64$ elements/radius. The numerator values (also shown in Table 1) suggest the precision of these denominator calculations is excellent.

Table 1: Integrals of distortions (Denominators) compared to errors (Numerators) normalized to far (ambient) values, calculated for N=64 Conformal Grid.

Insulating Sphere			Conducting Sphere	
Denominator	Numerator	For	Denominator	Numerator
35160.98 R^3	1.68 R^3	$\phi \,/\, E_{far}R$	35233.22 R^3	1.73 R^3
0.827621 R^3	$1.13 \times 10^{-4}R^3$	$J \,/\, J_{far}$	3.310526 R^3	$4.52 \times 10^{-4}R^3$
0.413132 R^3	$1.13 \times 10^{-4}R^3$	$E \,/\, E_{far}$	1.652572 R^3	$4.51 \times 10^{-4}R^3$
0.936859 R^3	$1.71 \times 10^{-4}R^3$	$J \cdot E \,/\, J_{far}E_{far}$	4.07748 R^3	$2.62 \times 10^{-4}R^3$

For the element-centered fields, the reference values normalized to far values squared (as shown in Table 1) can be interpreted as characteristic volumes for the octant modelled. Notice they are of order 1 – large fractions or a few R^3. No similarly intuitive interpretation for the ϕ denominator is apparent. There is no finite "far" value for ϕ; we chose $E_{far}R$ somewhat arbitrarily.

There is one set of references for an insulating sphere and another for a conducting sphere. The denominator values are the same for either the conformal or the brick grids for all resolutions. The values in Table 1 are the most accurate estimates. Hence, we used the same set of denominator values.

With this framework, the convergence of the global error is studied for spatial refinement of the Conformal and Brick meshes from $N = 8$ to $N = 64$. Using the Table 1 denominator values for all resolutions, the ranges of all relative error norms fall in comparable decades. Convergence plots for conducting spheres are shown in Figure 7. Results for the conformal grid are on the left, brick grid on the right. Convergence plots for insulating spheres are shown in Figure 8 in the same format.

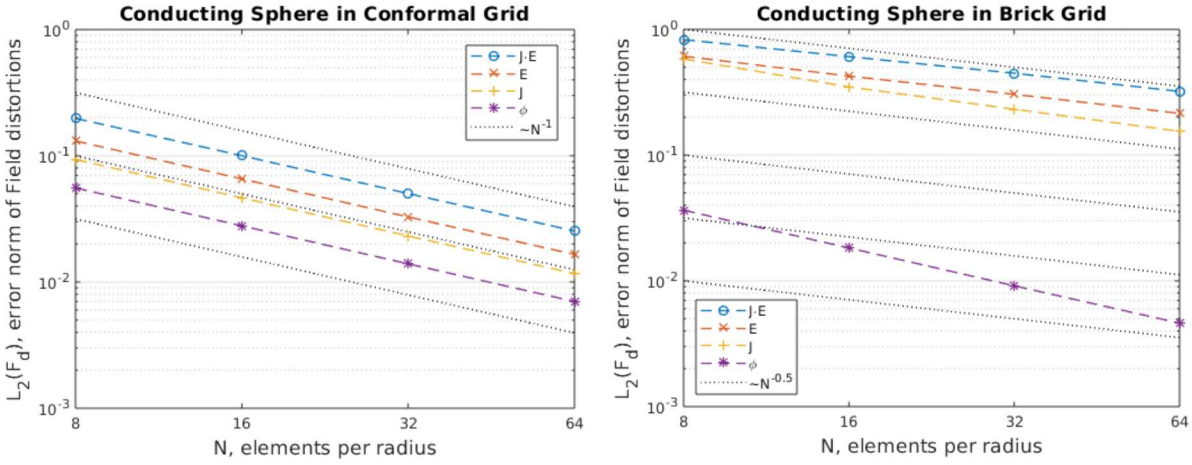

Figure 7: Convergence of global error norm for Conducting Sphere.

By inspection of the convergence plots in Figure 7 and Figure 8, it is apparent that the use of the Brick grid, with its mixed-material elements, strongly degrades both the accuracy of the solution at each resolution, and the rate of convergence over all resolutions. For all fields except the electric

potential, error magnitudes are roughly 10× larger, and the convergence rate drops from roughly 1 (the ideal value) to roughly 0.5. Also, at the coarsest mesh resolutions, the error in the electric field and Joule power is enormous – approaching the "far" values themselves.

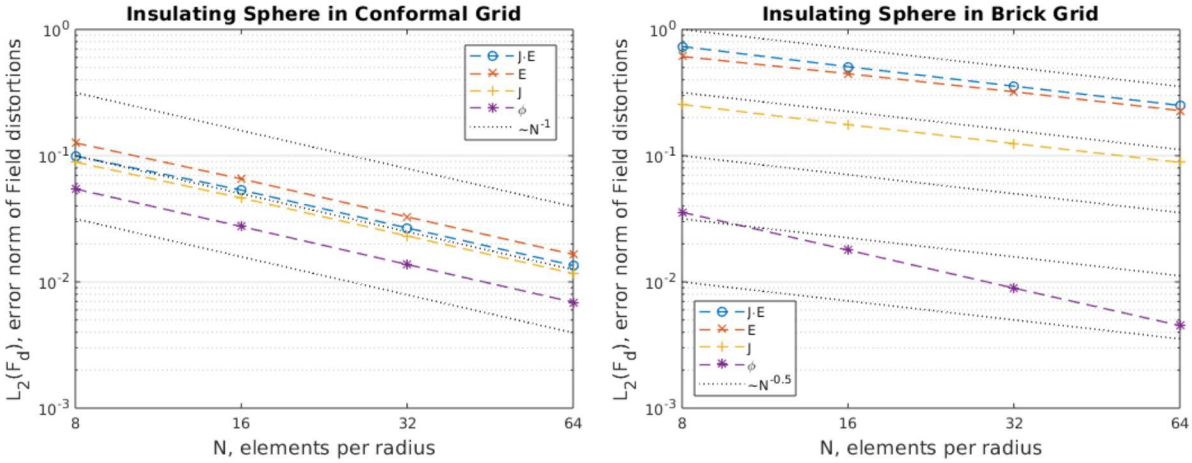

Figure 8: Convergence of global error norm for Insulating Sphere.

The slopes between pairs of resolution (factors of 2 apart) yield the actual convergence rates, which are listed in Table 2. The errors converge monotonically for all cases.

Table 2: Convergence rates for global error norm.

Conducting sphere in Conformal grid					Conducting sphere in Brick grid				
Res	ϕ	$\vec{J}$	$\vec{E}$	$J{\cdot}E$	Res	ϕ	$\vec{J}$	$\vec{E}$	$J{\cdot}E$
8/16	0.9970	1.0103	1.0000	0.9826	8/16	0.9976	0.7395	0.5254	0.4498
16/32	0.9993	1.0025	0.9999	0.9953	16/32	1.0004	0.5905	0.4813	0.4386
32/64	0.9924	0.9889	0.9882	0.9859	32/64	0.9870	0.5838	0.5044	0.4801
Insulating sphere in Conformal grid					Insulating sphere in Brick grid				
Res	ϕ	$\vec{J}$	$\vec{E}$	$J{\cdot}E$	Res	ϕ	$\vec{J}$	$\vec{E}$	$J{\cdot}E$
8/16	0.9891	0.9456	0.9496	0.8966	8/16	0.9978	0.5326	0.4530	0.5333
16/32	0.9992	0.9990	0.9997	0.9972	16/32	0.9995	0.4979	0.4757	0.5121
32/64	0.9927	0.9882	0.9882	0.9874	32/64	0.9862	0.4968	0.4960	0.5072

Several options were exercised in the ALEGRA code to determine if better results could be obtained for the Brick grid cases. These included a scheme that adjusts the electrical conductivity of mixed-material elements to account for the orientation of $\vec{E}$ with respect to the subgrid, reconstructed material interface [19]. None of these options improved or significantly changed the error magnitudes or convergence rates.

5.4. Sphere interior error analysis

As an alternative metric for solution accuracy, we can limit error norm calculations to the sphere interior. Inside the sphere, the exact fields are uniform, so the denominator calculation is trivial. We prefer to normalize errors to the analytical values in the sphere interior, e.g. $E_{in} = 1.5E_{far}$ for an insulating sphere and $J_{in} = 3J_{far}$ for a conducting sphere.

In Equation 5.1, the numerator has units of F^2 times volume, and the denominator reduces to the analytical value squared times volume. We compute the interior error norm as

$$L_2\left(\frac{F}{F_{in}}\right) = \sqrt{\frac{\int_{in} (F_{calc} - F_a)^2 dV}{F_{in}^2 V_{in}}} \tag{5.7}$$

where the numerator is evaluated discretely as before, but the denominator is now trivial. The interior L_2 errors for Conformal grids are seen in Figure 9. The errors normalized by analytical inside values are identical for $\vec{E}$ and $\vec{J}$, since they are exactly related by conductivity. Joule heating errors normalized by analytical inside values are comparable, even though the numerators are very small ($\sim 10^{-18}$).

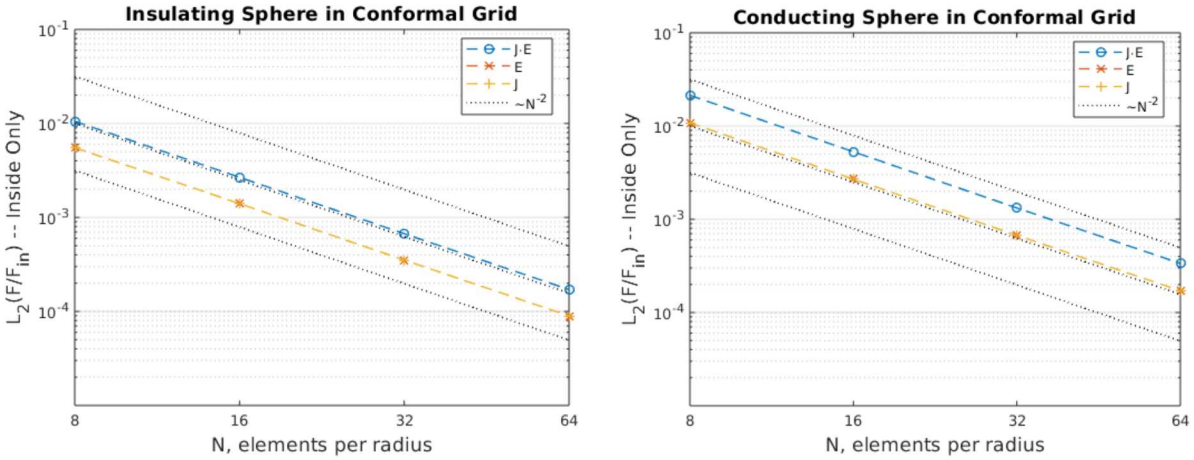

Figure 9: Volume-average interior error norms relative to interior solution for Conformal Grids.

For Brick grids, we considered any element with non-zero volume fraction of sphere material to be "inside," thus including all mixed-material elements. Those partial errors are dominated by the mixed-material elements, so we chose a different normalization. The enhanced interior field values ($1.5\times$ the "far" value for the insulating sphere, $3\times$ the "far" value for the conducting sphere) are also the maximum values just outside the sphere. (See Figure 3.) If we normalize by the maximum values, even for nominally negligible fields, we get a meaningful, comparable error metric for Joule heating errors. So, we define the error norm relative to maximum field values as follows:

$$L_2\left(\frac{F}{F_{max}}\right) \equiv \sqrt{\frac{\int_{in} (F_{calc} - F_a)^2 \, dV}{F_{max} V_{in}}} \tag{5.8}$$

The results are shown in Figure 10 for Brick grids. Because we use the error norm relative to the maximum field value for Brick grids, all three curves are again numerically comparable. Otherwise, the curves for $\vec{J} \cdot \vec{E}$ and either $\vec{J}$ or $\vec{E}$ would be 9 decades higher.

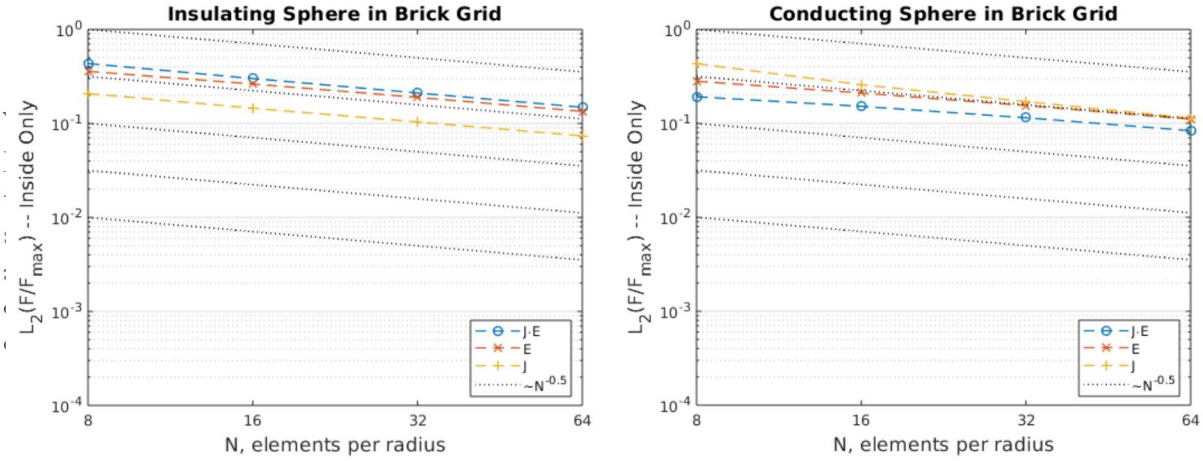

Figure 10: Volume-average interior error norms relative to maximum field values for Brick grids.

5.5. A closer look at mixed elements

To gain a clearer understanding of the nature of errors in mixed-material elements on Brick grids (which are typical of end-user simulations), we examine these errors using scatter plots. Scatter plots showing individual elements at slant ranges near $\rho = 1$ are obtained from the low-resolution cases, for easier visualization.

What should we compare these to? The analytical values at element centers would resemble step-functions for $\rho < R$ versus $\rho > R$. A more reasonable reference for comparing discrete values in mixed elements is the volume average of the analytical values in the mixed elements. We estimate those using volume fractions as weights applied to the interior and exterior formulas. (We use the element center location for the major portion, but we limit ρ/R to ≤ 1 or ≥ 1, respectively, to avoid evaluations on the "wrong" side.) The "interior" and "exterior" labels refer to values in either material separately. For $\vec{J}$ and $\vec{E}$, we approximate the volume integral of the exact solution in each element by forming a volume-weighted sum of the interior and exterior solutions. Because the volume fractions vary between 0 and 1 for mixed elements ($\rho \approx 1$), these reference values are continuous, intermediate values. They are plotted as green points in Figures 11-13, to provide a visual "sanity check" of the calculated values.

Figure 11 compares the x-components the current density vector computed by ALEGRA to the estimated volume averages of the analytical solution. (The transverse components are smaller except in small areas.) We see that ALEGRA current density in the mixed elements is reasonable for the insulating sphere, but noticeably distorted for the conducting sphere. On the right-hand plot, ALEGRA over-estimates J_x even in pure elements inside the sphere, and under-estimates it in most pure elements just outside.

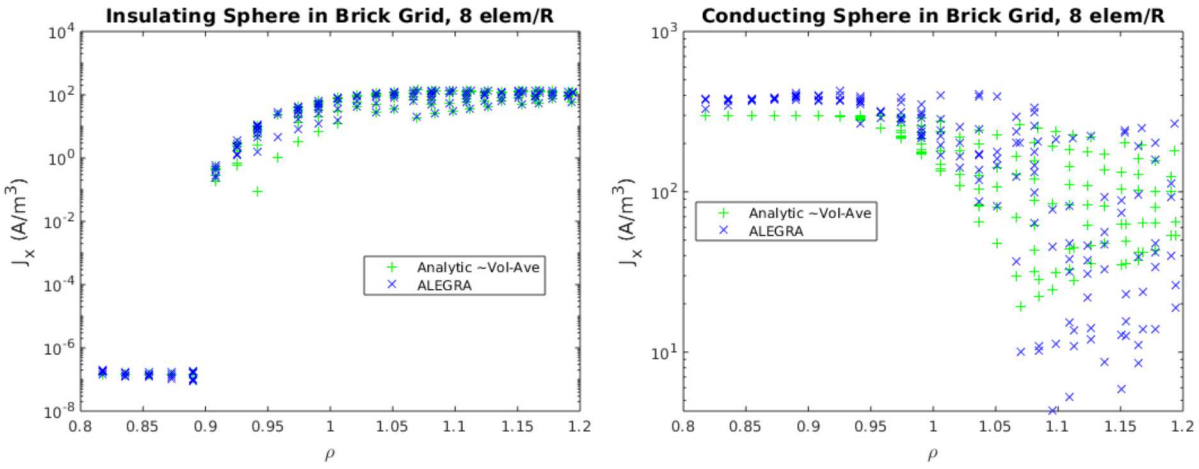

Figure 11: ALEGRA element-centered current density compared to volume-averages of analytical values in mixed elements.

Figure 12 compares the x-components of the electric field vector computed by ALEGRA to the estimated volume averages of the analytical solution. For the insulating sphere, ALEGRA's discrete values are lower than the volume averages in the mixed elements. For the conducting sphere, the discrete values are many orders of magnitude lower than the volume-averages.

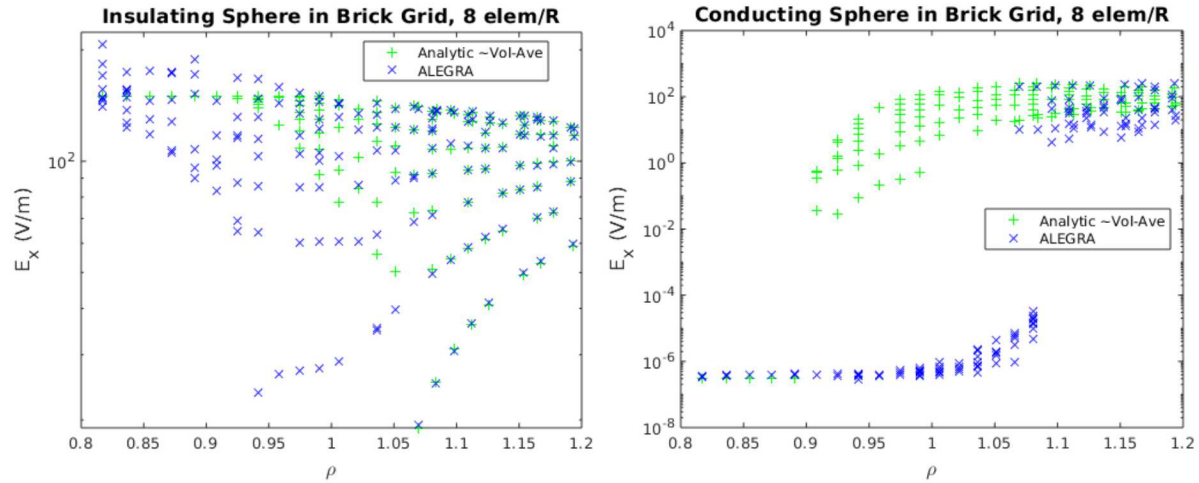

Figure 12: ALEGRA element-centered E-field compared to volume-averages of analytical values in mixed elements.

For $\vec{J} \cdot \vec{E}$, we keep the interior and exterior components separate to compare with ALEGRA calculated Joule heating in each material. In Figure 13, we see that the ALEGRA interior and exterior values for $\vec{J} \cdot \vec{E}$ are comparable to the analytical estimates for the insulating sphere, but not for the conducting sphere. For the latter, the estimated analytical values for $\vec{J} \cdot \vec{E}$ interior and exterior to the sphere are less than or equal to $9\, J_{far} E_{far}$ outside the sphere, and a small constant $\sim 10^{-4}$ inside, as expected. The calculated Joule power in the sphere interior is close to the expected value for $\rho < 1$, but increases by as many as eight orders of magnitude for $\rho > 1$—a significant over-estimation of conductor heating where its volume fraction is small. The calculated exterior heating is seriously under-estimated in the mixed elements, but reasonable orders of magnitude for pure exterior-material elements at $\rho > 1.1$. Furthermore, the total Joule heating in the mixed elements is underestimated by many orders of magnitude.

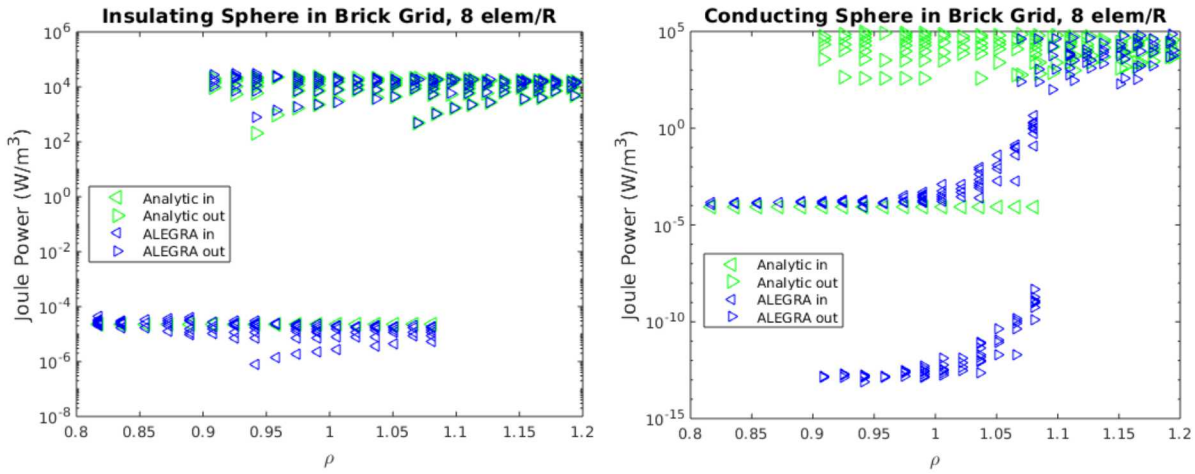

Figure 13: Interior and exterior Joule power computed by ALEGRA, compared to analytical values weighted by volume fraction.

We believe this reveals fundamental issues with ALEGRA's mixed-cell MHD model. This might relate to the absence of continuity conditions at material interfaces. Alternatively, it might have to do with the relationship between the electrical conductivity and the relative volume fractions of materials in mixed elements. Advanced techniques and/or discretizations need to be developed to overcome this, and concepts such as the "network linkage" concept of Reference [20] may need to be considered. As mentioned in Section 5.3, some advanced techniques already available in ALEGRA have been used here, to no avail. We anticipate further research into this area as development of ALEGRA and other MHD models continues into the future.

6. CONCLUSIONS

We have presented a verification study conducted for the ALEGRA software on a problem of an electrified medium with a spherical inclusion. The numerical solution on a conformal mesh at high resolution is visually indistinguishable from the exact solution. The maximum errors are near the interface, even for the conformal mesh. On a brick mesh, however, mixed-material elements introduce large errors that dominate global error norms. We have demonstrated that the electric field, current density and Joule power all converge at first order on a conformal mesh and at order one half on a brick mesh, which introduces mixed-material elements, while the electric potential converges at first order on both meshes. Analysis of errors limited to inside the sphere show the same convergence rates, except for potential—it converges to order one half on a brick mesh. We have also looked in detail at the field values which exist in the mixed-material cells, noting rough agreement with element volume-averages of the analytic solution in the insulating inclusion case, but orders-of-magnitude local differences from the analytic solution in the conducting inclusion case.

REFERENCES

[1] Robinson, AC, Brunner, TA, Carroll, S, and coauthors, "ALEGRA: An arbitrary Lagrangian-Eulerian multimaterial, multi-physics code." In: Proc. 46th AIAA Aerospace Sciences Meeting: AIAA-2008-1235, 2008.

[2] Doney, RL, Vunni, GB, and Niederhaus, JHJ, "Experiments and simulations of exploding aluminum wires: validation of ALEGRA-MHD," CCDC Army Research Laboratory Report ARL-TR-5229, 2010.

[3] Lemke, RW, Knudson, MD, Bliss, DE, Cochrane, K, Davis, J-P, Giunta, AA, Harjes, HC, and Slutz, SA, "Magnetically-accelerated, ultrahigh velocity flyer plates for shock wave experiments," *J. App. Phys.* **98**, 073530, 2005. https://doi.org/10.1063/1.2084316

[4] Kramer, RMJ, Bochev, PB, Siefert, CM, and Voth, TE, "Algebraically constrained extended edge element method (eXFEM-AC) for resolution of multi-material cells," *J. Comp. Phys.*, **276**, 596-612, 2014. https://doi.org/10.1016/j.jcp.2014.07.021

[5] Kramer, R, Bochev, P, Siefert, C, and Voth, T, "An extended finite element method with algebraic constraints (XFEM-AC) for problems with weak discontinuities," *Comp. Method. Appl. M.,* **266**, 70-80, 2013. https://doi.org/10.1016/j.cma.2013.07.013

[6] Grinfeld M, Niederhaus J, Porwitzky A. "Using the ALEGRA code for analysis of quasi-static magnetization of metals," CCDC Army Research Laboratory Report ARL-TR-7415, 2015.

[7] Grinfeld M, Niederhaus J. "ALEGRA-MHD simulations for magnetization of an ellipsoidal inclusion," CCDC Army Research Laboratory Report ARL-TR-8092, 2017.

[8] Grinfeld, M., Grinfeld, P., Niederhaus, JHJ, and Rodriguez, AE, "Electroconducting sphere inside bounded isotropic matrix for ALEGRA verification," CCDC Army Research Laboratory Report ARL-TR-8994, 2020.

[9] Elliott, CM and Larsson, S, "A finite element model for the time dependent Joule heating problem," *Math. Comp.* **64**(212), 1433-1453, 1995. https://doi.org/10.1090/S0025-5718-1995-1308451-4

[10] Holst, MJ, Larson, MG, Målqvist, and Söderlund, R, "Convergence analysis of finite element approximations of the Joule heating problem in three spatial dimensions," *BIT Numer. Math.* **50**, 781-795, 2010. https://doi.org/10.1007/s10543-010-0287-z

[11] Rienstra SW, "Geometrical effects in a Joule heating problem from miniature soldering," *J. Eng Math.* **31**, 59–80, 1997. https://doi.org/10.1023/A:1004281725734

[12] Robinson, AC, Petney, SV, and Garasi, CJ., "A low magnetic Reynolds number approximation for MHD modeling," Sandia National Laboratories unpublished draft report, 2013.

[13] Robinson, AC, Drake, RR, Luchini, CB, and Petney, SV, "Electromagnetic continuum mechanics in ALEGRA," Sandia National Laboratories unpublished manuscript., 2016.

[14] Siefert C, "Low Rm MHD for Alexa in one page," Sandia National Laboratories unpublished draft memo, 2017.

[15] Connors, J, "Convergence analysis and computational testing of the finite element discretization of the Navier–Stokes alpha model," *Numer. Meth. Part. D. E.* **26**(6), 1328-1350, 2010. https://doi.org/10.1002/num.20493

[16] Roy, CJ, Nelson, CC, Smith, TM, and Ober, CC, "Verification of Euler/Navier-Stokes codes using the method of manufactured solutions," Int. J. Numer. Meth. Fl. 44, 599-620, 2004. https://doi.org/10.1002/fld.660

[17] Roache, PJ, *Verification and Validation in Computational Science and Engineering*, Hermosa Publishing, 1998.

[18] Love, E and Wong, MK, "Lagrangian Continuum Dynamics in ALEGRA," Sandia National Laboratories technical report SAND2007-8104, 2007.

[19] Meredith, LT, Siefert, CM, Kramer, RMJ, "Interface based conductivity: an FEM approximation of electrical conductivity in multi-material cells," in Center for Computing Research Summer Proceedings, Sandia National Laboratories, 2016.

[20] Segletes, SB, "A model for the electrical conductivity of a mixed computational cell," CCDC Army Research Laboratory technical report ARL-TR-8979, 2020.

DISTRIBUTION

Email—Internal

Name	Org.	Sandia Email Address
Technical Library	01177	libref@sandia.gov

This page left blank.

Sandia National Laboratories

Sandia National Laboratories is a multimission laboratory managed and operated by National Technology & Engineering Solutions of Sandia LLC, a wholly owned subsidiary of Honeywell International Inc. for the U.S. Department of Energy's National Nuclear Security Administration under contract DE-NA0003525.